Available online at www.sciencedirect.com
SCIENCE DIRECT®
Scripta Materialia 53 (2005) 367–371
Scripta MATERIALIA
www.actamat-journals.com

Platelet microstructure and magnetic properties in rapidly solidified $Sm_{20.8}Co_{63.4}Fe_{7.9}Cu_{2.4}Zr_{1.6}B_4$ ribbons

R. Gopalan *, T. Ohkubo, K. Hono

National Institute for Materials Science, 1-2-1 Sengen, Tsukuba 305-0047, Japan

Received 16 March 2005; accepted 29 March 2005
Available online 29 April 2005

Abstract

The platelet microstructure observed in melt-spun $Sm_{20.8}Co_{63.4}Fe_{7.9}Cu_{2.4}Zr_{1.6}B_4$ ribbons that exhibit large coercivity has been characterized by transmission electron microscopy. The Sm_2Co_7 platelet disappears on annealing which causes a reduction in the coercivity ($_iH_c$).

Keywords: Melt-spinning; Microstructure; Hard magnets; Coercivity; SmCo

1. Introduction

The research interest in SmCo based permanent magnets has recently been revived in view of their potential applications at elevated temperatures [1–3]. Although commercial SmCo based magnets are produced by the powder metallurgy route with complicated heat treatments, a melt-spinning process is now being established as a viable processing route to develop high coercive SmCo magnets [4,5]. Obtaining high coercivity is not the only criteria, but also high remanence is required to achieve a high energy product $(BH)_{max}$. This has lead to an intense search for new compositions for improved magnet performance. Since $SmCo_5$ (1:5) has a higher magnetic anisotropy field than its counterpart Sm_2Co_{17} (2:17), it can be a suitable base composition to derive new compositions with minor alloying additions [6]. With modified compositions, one may not necessarily achieve a $Sm_2Co_{17}/SmCo_5$ nanocomposite microstructure as in the commercial $Sm(Co, Fe, Cu, Zr)_{7.5}$ magnets, but may strike different microstructures that could improve the magnetic properties.

In our previous studies, we investigated microstructure–magnetic property relationships in a series of $Sm(Co, Cu, Fe, Zr, B)_x$ melt-spun ribbons with $x \approx 7$–12 [7,8]. The Sm–Co, Sm–Co–Cu and Sm–Co–Fe phase diagrams in combination with the structure types of Sm_xCo_y phases were taken as the tools to design these compositions. The coercivity mechanism of these melt-spun ribbons was discussed based on the size effect as well as on the formation of the $TbCu_7$ type structure [7,8]. In the present study, we have selected a composition of $Sm_{20.8}Co_{63.4}Fe_{7.9}Cu_{2.4}Zr_{1.6}B_4$, with $x = 4.8$ in the $Sm(Co, Cu, Fe, Zr, B)_x$ formula. The Fe substitution for Co in the composition is expected to enhance the magnetic moment of the hard magnetic phase, while Zr and B will help in refining the microstructure. The purpose of this work was to look at the microstructural changes in this typical composition on rapid quenching and annealing, and to understand the associated variation of the hard magnetic properties.

2. Experimental

Rapidly solidified ribbons with a nominal composition of $Sm_{20.8}Co_{63.4}Fe_{7.9}Cu_{2.4}Zr_{1.6}B_4$ were prepared at

* Corresponding author.
E-mail address: raghavan.gopalan@nims.go.jp (R. Gopalan).

1359-6462/$ - see front matter
doi:10.1016/j.scriptamat.2005.03.050

different wheel surface speeds with the single roller melt-spinning method. To study the effect of annealing, the ribbons were heat-treated at 773–873 K in vacuum. The constituent phases of the ribbons were identified by X-ray diffraction (XRD) using CuK_α radiation. The microstructures of the ribbons were characterized using a Philips CM 200 transmission electron microscope (TEM). The nanobeam diffraction (NBD) for the phase identification and energy dispersive X-ray spectroscopy (EDS) for a qualitative chemical analysis of the constituent phases were carried out by using a JEOL 2010F TEM. Magnetic properties of the samples were measured in the plan direction of the ribbon samples using a vibrating sample magnetometer (VSM).

3. Results

Fig. 1 shows the XRD patterns for $Sm_{20.8}Co_{63.4}Fe_{7.9}Cu_{2.4}Zr_{1.6}B_4$ ribbons melt-spun at various wheel surface speeds (5, 10 and 15 m/s). The predominant phase in the ribbons melt-spun at 15 m/s has the $TbCu_7$ (1:7) type structure. At 10 m/s wheel surface speed, the main phase in the ribbons is $SmCo_5$ phase with the $CaCu_5$ type structure and with small traces of Sm_2Co_7 (2:7). With a further decrease of the wheel surface speed to 5 m/s, the 2:7 phase appears to be dominant together with a small fraction of the 1:5 phase. The relative intensity of the $(0\,0\,2)_{1:5}$ peak is intense (Fig. 1b), indicating the development of some preferred $(0\,0\,l)$ texture in the ribbons melt-spun at 10 m/s. The $(0\,0\,l)$ direction of the 1:5 phase is the easy axis of the magnetization.

We also investigated the effect of the heat treatment on the $Sm_{20.8}Co_{63.4}Fe_{7.9}Cu_{2.4}Zr_{1.6}B_4$ ribbons. The ribbons were annealed in a vacuum at temperatures of 773, 823 and 873 K for 10 min. The heat treatment caused the 10 m/s ribbons to crystallize into nearly the single phase 1:5 with almost no trace of the 2:7 phase. A typical XRD pattern of 10 m/s ribbon annealed at 823 K is shown in Fig. 1d. The heat treatment did not alter the structure of the ribbons melt-spun at 5 and 15 m/s and still the 2:7 and 1:7 phases were retained as major phases, respectively.

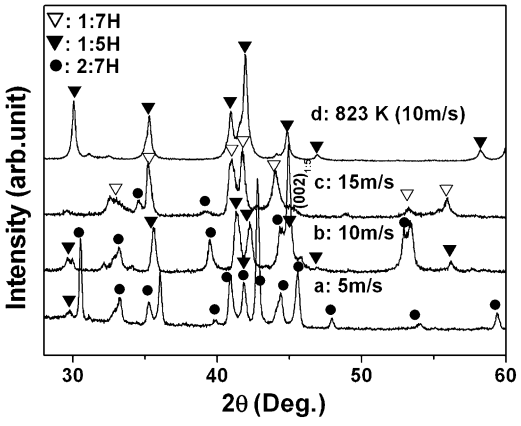

Fig. 1. XRD patterns for the as-spun ribbons of $Sm_{20.8}Co_{63.4}Fe_{7.9}Cu_{2.4}Zr_{1.6}B_4$: (a) 5 m/s, (b) 10 m/s and (c) 15 m/s. The (0 0 2) peak of the 1:5 phase is intense for the ribbon of 10 m/s.

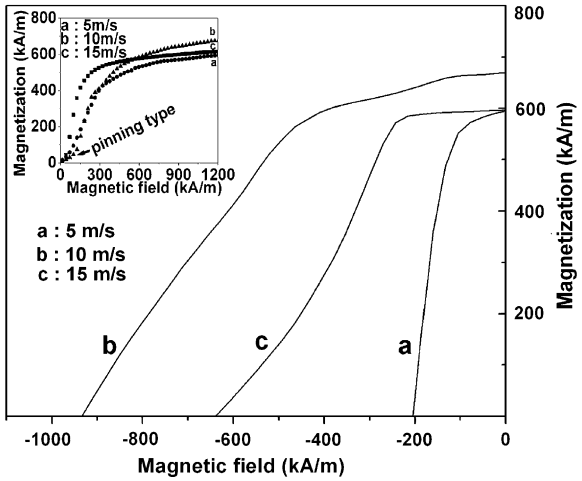

Fig. 2. Demagnetization curves for $Sm_{20.8}Co_{63.4}Fe_{7.9}Cu_{2.4}Zr_{1.6}B_4$ ribbons melt-spun at (a) 5 m/s, (b) 10 m/s and (c) 15 m/s. The corresponding initial magnetization curves are shown in the inset.

Fig. 2 shows the demagnetization curves for the as-spun ribbons of $Sm_{20.8}Co_{63.4}Fe_{7.9}Cu_{2.4}Zr_{1.6}B_4$ for different wheel surface speeds. The inset to Fig. 2 shows the typical initial magnetization curves of the corresponding ribbons. The ribbon melt-spun at 5 m/s has a coercivity ($_iH_c$) of 200 kA/m (2.5 kOe) while the ribbon melt-spun at higher wheel surface speeds (10 and 15 m/s) has $_iH_c > 640$ kA/m (8 kOe) with a maximum of 930 kA/m (11.6 kOe) at 10 m/s. The coercivity is low for 5 m/s ribbons due to the formation of the 2:7 phase which has a low magnetocrystalline anisotropy [9]. The ribbon melt-spun at 10 m/s has a high $_iH_c$ of 930 kA/m (11.6 kOe) and this is due to the coexistence of the 2:7 phase with the 1:5 phase (Fig. 1b). This is also further supported by the initial magnetization curves shown in the inset to Fig. 2. The initial magnetization curves of 5 m/s and 15 m/s ribbon show a sharp rise of the magnetization even at a lower magnetic field, which is an indication of the nucleation type coercivity mechanism, while that of 10 m/s ribbon showed dragging of the curve, typical for the pinning type mechanism [10]. We did not observe any step in the demagnetization curves for all the ribbons, which would have suggested the existence of the magnetically softer phase such as α-Fe or Fe(Co) or their borides. The remanence (M_r) values for 5, 10 and 15 m/s ribbons are 592, 674 and 598 kA/m, respectively. The higher remanence at 10 m/s wheel surface speed could be an outcome of some preferred texture as evidenced from the XRD results (Fig. 1b). The corresponding $(BH)_{max}$ of the samples were estimated to be